Perpendicular magnetic anisotropy via strain-engineered oxygen vacancy ordering in epitaxial $La_{1-x}Sr_{x}CoO_{3-\delta}$

Jeff Walter, Shameek Bose, Mariona Cabero, Guichuan Yu, Martin Greven, Maria Varela, and Chris Leighton

Phys. Rev. Materials **2**, 111404 — Published 19 November 2018

DOI: 10.1103/PhysRevMaterials.2.111404

Revised version resubmitted to *Phys. Rev. Materials* as a *Rapid Communication* on 10/26/2018

Perpendicular Magnetic Anisotropy *via* Strain-Engineered Oxygen Vacancy Ordering in Epitaxial $La_{1-x}Sr_xCoO_{3-\delta}$

Jeff Walter,[1] Shameek Bose,[1] Mariona Cabero,[2] Guichuan Yu,[3] Martin Greven,[2] Maria Varela,[2] and Chris Leighton[1]*

[1]*Department of Chemical Engineering and Materials Science, University of Minnesota, Minneapolis, MN 55455*

[2]*Dept. de Física de Materiales & Instituto Pluridisciplinar, Universidad Complutense de Madrid, 28040 Madrid, Spain*

[3]*School of Physics and Astronomy, University of Minnesota, Minneapolis, MN 55455*

Abstract: Tuning oxygen vacancy concentrations is a well-established approach to controlling properties of complex oxides. Recent work on perovskite cobaltites has shown that *ordering* of oxygen vacancies can also be tuned, *via* heteroepitaxial strain, presenting new opportunities. Here we demonstrate that strain-engineered vacancy ordering can control and enhance magnetic anisotropy in $La_{1-x}Sr_xCoO_{3-\delta}$. In particular, *in-plane* oxygen vacancy order induced by compressive strain is shown to result in remarkably strong *perpendicular* magnetic anisotropy, with anisotropy constant up to 6×10^6 erg/cm^3. The anisotropy is thickness-independent, ruling out surface and film/substrate interface anisotropy, but strongly correlated with lateral coherence of defect order from electron microscopy. The results are discussed in terms of the unit-cell-level superlattice induced by the oxygen vacancy order, generating intriguing analogies with metal-based multilayer systems. Generally, this work highlights the significant potential of strain-based manipulation of oxygen vacancy ordering to control and enhance complex oxide properties.

*Corresponding author: leighton@umn.edu

SECTION: Magnetic, ferroelectric, and multiferroic materials

PHYSH: Research Areas: Magnetic anisotropy
Physical Systems: Heterostructures, Oxides

Complex oxide heterostructures offer a vast playground for new materials science, physics, and chemistry, with much appeal in science and technology [1–5]. ABO_3 perovskites are of particular interest in this context, due to extraordinary chemical flexibility, diverse functionality, and lattice matching capability [1–5]. Perovskite heterostructures have thus enabled numerous discoveries, such as new interfacial phenomena (*e.g.*, two-dimensional electron gases at insulator/insulator interfaces [2,5,6]), strain-stabilized non-equilibrium states (*e.g.*, ferroelectricity in paraelectric materials [7,8]), and electric-field-tuned insulator-metal-superconductor transitions [9,10]. Existing or potential applications are thus abundant, in ferroelectric random access memory, resistive memory, solid oxide fuel cells, catalysis, and oxide electronics in general [1–5]. Tuning of oxygen non-stoichiometry, *i.e.*, δ in $ABO_{3\pm\delta}$, is a particularly powerful means to control perovskites. Enthalpies of formation of oxygen vacancies (V_O), for example, are frequently low, enabling tuning of δ in $ABO_{3-\delta}$ *via* thermal treatment [11–16] or electric fields [17–20], often reversibly [11,12,16–18]. Due to the impact of δ on doping, and thus electronic, magnetic, and optical properties, such stoichiometry tuning is highly effective for control of function [11–20].

In many $ABO_{3-\delta}$ perovskites, the V_O are essentially randomly located, *i.e.*, disordered. In some, however, oxygen vacancy *ordering* occurs, the V_O crystallizing into short- or long-range structures. $SrCoO_{3-\delta}$ provides a prototypical example [21–23]. The cubic perovskite structure is maintained in this compound to only modest δ (0.125-0.25 [21,23]), beyond which oxygen-vacancy-ordered (OVO) phases occur, most notably orthorhombic brownmillerite $Sr_2Co_2O_5$ [21–23]. The latter is a defect-ordered form of $SrCoO_{2.5}$ (*i.e.*, $SrCoO_{3-\delta}$ with $\delta = 0.50$), derived from $SrCoO_3$ by forming V_O in lines along the [101] cubic direction, in alternating (100) planes, creating the superlattice in Fig. 1(a) [22]. This results in alternating octahedrally- and

tetrahedrally-coordinated Co, as shown in Fig. 1(a), and a decrease in formal valence from 4+ to 3+ [21–23]. The instability of Co^{4+} is in fact a key factor in the relative stability of brownmillerite $SrCoO_{2.5}$, similar to other OVO compounds such as $CaFeO_{2.5}$ [24]. Illustrating this, at typical bulk synthesis temperatures, O_2 pressures of hundreds of atmospheres are required to decrease δ to the point that perovskite $SrCoO_{3-\delta}$ is stabilized over brownmillerite $SrCoO_{2.5}$ [25]. As δ is tuned in $SrCoO_{3-\delta}$, multiple OVO superstructures occur, at $\delta \approx 1/8$, 1/4, 1/2, with very different properties [23]. Cubic $SrCoO_3$ is a ferromagnetic (F) metal with Curie temperature $T_C \approx 305$ K [25], for example, whereas orthorhombic brownmillerite $SrCoO_{2.5}$ is an insulating (2.1 eV band gap) antiferromagnet (AF) [17].

In light of the above, the ability to precisely tune V_O *order*, in addition to V_O *concentration*, would provide unique opportunities. Recent publications report exciting progress in this direction. Reversible topotactic transformations between perovskite $SrCoO_{3-\delta}$ and brownmillerite $SrCoO_{2.5}$ have been demonstrated in films, for example, driven by controlled atmosphere annealing (at mildly elevated temperatures) [11,12], as well as electrolyte gating (at modest voltages, even near room temperature) [17,26]. Metal-insulator and F-AF phase transitions have been thus controlled, with wide dynamic range in resistivity and magnetization (M) [11,12,17]. It is therefore established that V_O order/disorder transitions can be driven by temperature- or electric-field-stimulated redox in cobaltites, *i.e.*, by tuning δ.

Complementary to this, our recent work on the related $La_{1-x}Sr_xCoO_{3-\delta}$ (LSCO) has demonstrated tuning, *via* heteroepitaxial strain, of the *orientation* of OVO superstructures [27,28]. This is enabled by a novel lattice mismatch accommodation mechanism in epitaxial LSCO, based on V_O order [27]. Specifically, when $x = 0.5$ LSCO (pseudocubic bulk lattice parameter, $a_{LSCO} = 3.83$ Å) films are grown under tension (*e.g.*, on $SrTiO_3$(001), $a_{STO} =$

3.91 Å), the lattice mismatch is accommodated by ordered oxygen-deficient planes oriented perpendicular to the interface [27,29], expanding the in-plane lattice parameter without misfit dislocations (Fig. 1(a)) [27]. In essence, the oxygen-deficient planes (light gray, Fig. 1(a)) have an expanded local lattice spacing compared to oxygen sufficient planes (red, Fig. 1(a)), the sum of the spacings matching twice the STO lattice parameter [27]. Conversely, under compression (*e.g.*, on $LaAlO_3$(001), a_{LAO} = 3.79 Å) the mismatch is accommodated by ordered oxygen-deficient planes *parallel* to the interface [27,29], *decreasing* the average in-plane lattice spacing (Fig. 1(b)) [27]. Importantly, unlike the $SrCoO_{3-\delta}$ discussed above [11,12,17,26], in this case $\delta < 0.5$, the brownmillerite-like ordering not being complete. At the $SrTiO_3$(001)/LSCO interface for example, $\delta \approx 0.13$, indicating *coexistence* of perovskite and brownmillerite structures [30]. This reflects the nominal Co valence of 3.5+ in $x = 0.5$ LSCO (compared to 4+ in $SrCoO_3$), increasing the relative stability of the perovskite phase.

The above mechanism couples lattice mismatch, strain, and V_O concentration in LSCO films, necessarily impacting electronic and magnetic properties. In $SrTiO_3$(001)/LSCO, for instance, the substantial δ required near the interface for V_O-order-based mismatch accommodation leads to lowering of the effective doping, $x_{eff} = x - 2\delta$ [28,31]. At thickness $t \approx$ 70 Å, x_{eff} is decreased from 0.5 to as low as 0.22, triggering a crossover from a uniform long-range-ordered F metal to a magneto-electronically phase-separated state with F clusters in a non-F insulating matrix [28], as expected from bulk behavior [32–34]. Strain-induced V_O order is thus the origin of the magnetic dead layer effect in LSCO, where M, T_C, and conductivity are suppressed in very thin films [28,31]. Coercivity (H_c) is similarly impacted. H_c in STO(001)/LSCO films is enhanced over bulk (up to 100-fold), increasing rapidly as t is reduced to the 70 Å dead layer thickness [35]. This is due to domain wall pinning by the magnetically-

phase-separated interfacial layer, maximizing H_C [35]. In all cases, the magnetization in $SrTiO_3$(001)/LSCO films retained typical in-plane orientation [28,31,35].

While strain-engineering of the orientation of OVO superstructures in epitaxial cobaltites is thus established, the impact of this orientation on magnetism remains unexplored. Tensile-strained LSCO on $SrTiO_3$(001) (with out-of-plane OVO superstructure, Fig. 1(a)), is in fact the only case studied in detail [28,31,35]. This is a notable void in the literature, particularly given the unique opportunity to understand how V_O-order-induced symmetry lowering could impact magnetism and transport. Here, we thus study the impact of tensile and compressive lattice mismatch on magnetism in thoroughly-characterized V_O-ordered LSCO epilayers. The results reveal typical in-plane magnetic anisotropy under tension, but *perpendicular* anisotropy under compressive strain, *i.e.*, when an *in-plane* OVO superstructure forms. Perpendicular magnetic anisotropy (PMA) is rare in perovskites, and occurs here with large anisotropy constant, up to 6 $\times$ 10^6 erg/cm^3. The PMA is *t*-independent, eliminating surface and interface anisotropies, but strikingly correlated with lateral coherence of V_O order from Transmission Electron Microscopy (TEM). An origin related to the unit-cell-level OVO superlattice is thus implicated, with intriguing parallels with conventional PMA systems such as ultra-short-period Co/Pt and Co/Ni multilayers.

Epitaxial LSCO films ($0.05 < x < 0.50$) were deposited *via* high-pressure-oxygen reactive sputtering at 600 °C, in 1.4 Torr of O_2, at 15 Å/min. Details on growth, and extensive characterization, have been published [19,20,28,30,31,35]. The substrates employed, with resulting in-plane lattice mismatches (and thus in-plane strains (ε_{xx}) if fully-strained to the substrate) were (001)-oriented $SrTiO_3$ (STO, 1.8%), $La_{0.18}Sr_{0.82}Al_{0.59}Ta_{0.41}O_3$ (LSAT, 0.8%), $LaAlO_3$ (LAO, -1.2%), and $SrLaAlO_4$ (SLAO, -2.1%); this spans from 1.8% tensile to 2.1%

compressive. Structural characterization was achieved through high-resolution Wide-Angle X-Ray Diffraction (WAXRD) at the Advanced Photon Source beamline 33-ID (using a six-circle Kappa-type goniometer, a Pilatus II 100K area detector, and 0.62 Å wavelength), as well as high-angle annular dark field (*Z*-contrast) cross-sectional scanning TEM (STEM). STEM data were acquired in a Cs aberration corrected JEOL ARM200cF operated at 200 kV. Cross-sectional samples were prepared by mechanical grinding, polishing, and Ar ion milling, in both pseudocubic [110] and [010] orientations. The final Ar cleaning used low voltage (0.5 kV) to avoid sample damage, while beam currents for imaging were kept in the 10's of pA range for the same reason. This is a known important issue in OVO cobaltites. Magnetometry was done in a Quantum Design MPMS from 5-300 K in magnetic fields (H) to 70 kOe. When in-plane, these fields were applied along substrate [100] directions.

Fig. 2(a-d) shows representative specular synchrotron WAXRD near the 002 reflections of 90-Å-thick x = 0.5 LSCO films on all four substrates. Well-defined 002 LSCO peaks occur, with clear Laue fringes, demonstrating (001)-oriented epitaxy and low roughness. Scherrer lengths from the 002 reflections of all films (85 ± 6 Å), agree with thicknesses from Laue fringes (86 ± 5 Å) and X-ray reflectivity (90 ± 6 Å). Out-of-plane lattice parameters (c_{op}) were extracted from LSCO peak positions to determine out-of-plane strains, $\varepsilon_{zz} = (c_{op} - a_{LSCO})/a_{LSCO}$. As shown in Fig. 2(e), the deduced ε_{zz} *vs.* ε_{xx} is linear, with a slope near -1, consistent with a Poisson ratio of 1/3; this is common in strained cobaltites, *e.g.*,[36]. A representative reciprocal space map around the 013 reflections of a 380-Å-thick x = 0.5 LSCO film on LAO is provided in Fig. 2(f), showing the film and substrate peaks, and multiple Laue fringes. The LSCO film peak occurs at identical $1/d_{010}$ to the substrate (the d_{hkl} here are lattice spacings), but at decreased $3/d_{001}$, confirming fully-strained pseudomorphic growth. The critical thickness for strain relaxation

varies with substrate, but is >380 Å (the maximum t studied here) for all substrates. All films in this work, on all substrates, are thus fully-strained, supported by reciprocal space maps (*e.g.*, Fig. 2(f)), thickness dependence of lattice parameters, and the behavior in Fig. 2(e) [27,28].

We begin the discussion of magnetic properties with the temperature (T) dependence of M for representative 90-Å-thick x = 0.5 LSCO films on STO, LSAT, LAO, and SLAO (Fig. 3(a-d). The two curves shown here are for out-of-plane (OoP, solid lines) and in-plane (IP, dashed lines) 1 kOe measuring and cooling fields. Films on STO and LSAT (*i.e.*, under tensile strain, Fig. 3(a,b)) exhibit the expected F behavior, with $T_C \approx 215$ K at this t [28] (as estimated from d^2M/dT^2), and in-plane M well in excess of out-of-plane M, indicating in-plane anisotropy. This is consistent with 5 K $M(H)$ loops on STO and LSAT (Fig. 3(e,f)), which, for in-plane H, reveal substantial H_c (up to 11.2 kOe) and remnant magnetization (M_r, up to 1.3 μ_B/Co, or 0.65M_s, where M_s is the saturation magnetization). Out-of-plane H instead results in negligible H_c and M_r, but large saturation fields up to ~70 kOe. $M(T)$ and $M(H)$ thus indicate clear in-plane magnetic anisotropy in tensile-strained x = 0.5 LSCO films, consistent with prior work [28,31,35,37].

Very different behavior is found on LAO and SLAO (*i.e.*, under compression, Fig. 3(c,d) and (g,h)). The expected F behavior is preserved, with a slightly enhanced $T_C \approx 221$ K on LAO, *but with perpendicular magnetic anisotropy*. This is evidenced by out-of-plane M exceeding in-plane M in $M(T)$ (Fig. 3(c,d)), as well as the largest H_c and M_r values occurring out-of-plane (Fig. 3(g,h)). Fig. 3(g), for LAO, in fact shows exemplary PMA, the out-of-plane M_r and H_c reaching 1.6 μ_B/Co (0.8M_s) and 6.1 kOe, while the in-plane $M(H)$ displays small H_c and large saturation field (36 kOe). This tendency to perpendicular magnetization under compression is maintained on SLAO (ε_{xx} = -2.1%), albeit with weaker PMA. In Fig. 3(h), for example, $M(H)$ in- and out-of-plane is similar, although H_c and M_r/M_s *are* larger out-of-plane. This indicates a perpendicular

component to the anisotropy on SLAO (compare Fig. 3(f and h), for example), but of insufficient strength to completely dominate the magnetocrystalline anisotropy and demagnetizing field. As a final comment on $M(H)$, note that in all cases (Fig. 3(e,f,g,h)), $M_s \approx 2\ \mu_B$/Co, as expected at this x and t [28,31].

A summary of the ferromagnetic properties of these 90-Å-thick $x = 0.5$ LSCO films is provided in Fig. 3(i-k), which plots the ε_{xx} dependence of T_C, H_c, and M_r/M_s. T_C (Fig. 3(i)) is relatively constant, but with a minor increase at negative ε_{xx}, previously ascribed to decreased average Co-O bond lengths [37]. The response of H_c and M_r/M_s to ε_{xx} is more striking (Fig. 3(j,k)), reflecting the clear transition from in-plane to perpendicular anisotropy. In essence, the relative in-plane and out-of-plane H_c values invert from $\varepsilon_{xx} > 0$ (in-plane M) to $\varepsilon_{xx} < 0$ (out-of-plane M). Correspondingly, M_r/M_s is largest for in-plane H at $\varepsilon_{xx} > 0$, but largest for out-of-plane H at $\varepsilon_{xx} < 0$. PMA under compressive strain is thus confirmed for $x = 0.5$ LSCO films. As noted, this PMA is slightly diminished at $\varepsilon_{xx} = -2.1\%$ (SLAO) compared to -1.2% (LAO). This may be a consequence of lower film quality at large strain, evidenced by slightly higher residual resistivity on SLAO than LAO (72 *vs*. 60 μΩcm).

These data enable quantitative estimation of an effective magnetic anisotropy constant, or energy density, K_{eff}. We first do this for the exemplary case in Fig. 3(g), *i.e*., LAO(001)/LSCO, with PMA. Assuming uniaxial anisotropy, K_{eff} can be estimated from the hard-axis (in-plane in this case) saturation field, *i.e*., the anisotropy field, H_a, using $K_{eff} \approx M_s H_a/2$ [38]. Estimating H_a as the point where $0.9M_s$ is reached in Fig. 3(g) (36 kOe) then gives $K_{eff} \approx 6.0 \times 10^6$ erg/cm^3. K_{eff} can also be estimated from the maximum H_c as a function of t, assuming Stoner-Wohlfarth behavior. This assumes the maximum H_c results from coherent magnetization rotation, giving $K_{eff} \approx (M_s H_{c,max})/2$ [35,38]. Using $H_c = 8$ kOe at $t = 35$ Å (Fig. 3(m)) then yields $K_{eff} \approx 1.5 \times 10^6$

erg/cm^3. Considering the latter is a lower bound [35], the two estimates are in good agreement. To put 6.0×10^6 erg/cm^3 in context, note that estimates for K_{eff} in *bulk* LSCO, which are already far larger than in manganites [35,39], lie at $0.3\text{-}2.1 \times 10^6$ erg/cm^3 [35,39,40]. Taking LSAT(001)/LSCO (Fig. 3(f)) as exemplary of *in-plane* anisotropy, the hard-axis saturation field (taking into account the demagnetizing field) gives $K_{eff} \approx M_s(H_a - 4\pi M_s)/2 \approx 7.0 \times 10^6$ erg/cm^3. K_{eff} is thus essentially constant at $6\text{-}7 \times 10^6$ erg/cm^3 in these LSCO films, 3-20 times higher than bulk, with clear rotation of the easy-axis from in-plane to perpendicular under compression. For context, note that, despite the absence of heavy elements, these anisotropy constants are only one order of magnitude below well-known high anisotropy ferromagnets such as $SmCo_5$ (7×10^7 erg/cm^3 at 4.2 K [38]).

Common origins of PMA in metal-based systems include surface and/or interface anisotropies that overcome magnetocrystalline anisotropies and demagnetizing fields with decreasing t [41,42]. A full t dependence (30-380 Å) was thus measured for $x = 0.5$ LSCO on LAO (Fig. 3(l-n)). T_C is constant above ~75 Å, below which it decreases, before plummeting near 25 Å (Fig. 3(l)). This is consistent with the dead layer critical thickness, t_c, for LAO(001)/LSCO which is 6 unit cells (23 Å) based on the metal-insulator transition and loss of the anomalous Hall effect [20,43]. t_c for $x = 0.5$ LSCO is thus substantially lower on LAO(001) than on STO(001) (18 unit cells) [28,31], as will be discussed elsewhere [44]. Significantly, the t dependencies of the 5 K H_c and M_r/M_s (Fig. 3(m,n)) are far weaker. The in-plane H_c increases by a factor of only 1.37 on decreasing t, while the out-of-plane H_c increases by only 1.57. The overall trend of H_c increasing as t is lowered is unsurprising [35], the important observation being the dominance of out-of-plane H_c over in-plane H_c at all t. Similarly, M_r/M_s remains 2-3 times larger out-of-plane than in-plane at all t, the decreases in M_r/M_s as $t \rightarrow t_c$ being expected,

due to the crossover from long-range F to nanoscopic F clusters [28]. Based on Fig. 3(l-n), PMA in LAO(001)/LSCO is thus maintained over a wide t range, with no indication of a crossover to in-plane anisotropy with increasing t, ruling out surface and/or film/substrate interface anisotropies. This qualitative t independence of anisotropy was found on all substrates.

With surface and/or substrate/film interface anisotropies ruled out, we next turn to x dependence for clues to the origin of the PMA under compression. Fig. 4(a-d) thus shows 5 K $M(H)$ loops for ~100-Å-thick LAO(001)/$La_{1-x}Sr_xCoO_{3-\delta}$ with x = 0.5, 0.28, 0.15 and 0.05. As x is lowered, M_s decreases, followed by H_c, eventually yielding a sheared, low H_c loop at x = 0.15 and 0.05. This is expected based on bulk crystals, where the F volume fraction falls from unity at x = 0.22, dropping rapidly at the percolation threshold, x_c = 0.18 [34]. More important here, however, is the anisotropy. The strong PMA at x = 0.5 diminishes at x = 0.28, although H_c and M_r/M_s remain larger out-of-plane (11.3 kOe and 0.25) than in-plane (6.1 kOe and 0.23), indicating a significant perpendicular component. At x = 0.15 and 0.05, however, below x_c, $M(H)$ becomes essentially isotropic. The PMA at high x, in the long-range F phase, thus disappears below x_c, as might be expected. Fig. 4(e-h) shows corresponding Z-contrast STEM. The x = 0.5 image (Fig. 4(e)) is as expected, the OVO superstructure being *in-plane*, as anticipated under compression [27,29]. At x = 0.28, however, the lateral coherence of V_O order is considerably reduced. Short (~10 nm) sections of oxygen-deficient planes (red arrows) are visible, but with antiphase boundaries and regions where V_O order is not apparent. At x = 0.15 the OVO contrast further decreases, becoming undetectable at x = 0.05. While quantification of OVO volume fraction from STEM is challenging [27,28,45], Fig. 4(e-h) nevertheless reveals a clear evolution with x, which can be simply rationalized. As x is decreased in Fig. 4 the nominal Co valence drops from 3.50+ to 3.05+, thus decreasing the concentration of V_O, along with the OVO volume

fraction. We note that OVO superstructures *have* been reported at $x = 0$, however [46,47], meaning that non-monotonic x dependence is possible. While surprising, this is in agreement with some magnetic data [48].

With respect to the *mechanism* for perpendicular anisotropy under epitaxial compression, we first note that PMA has also been reported in some compressively-strained $La_{1-x}Sr_xMnO_3$ films [49,50]. This was ascribed to a bulk magnetostrictive mechanism, based on opposite signs of longitudinal (positive) and transverse (negative) magnetostrictions [49,51]. While the magnetocrystalline anisotropy to overcome is over an order-of-magnitude larger in LSCO [35,39,40], magnetostrictions are also approximately an order-of-magnitude larger [51,52], making this a significant potential factor. The obvious symmetry lowering due to V_O order, however, cannot be ignored in LSCO. Fig. 4 in fact exposes clear correlations between the OVO superstructure and PMA in LAO(001)/$La_{1-x}Sr_xCoO_{3-\delta}$. The $x = 0.28$ data are particularly important here, as at $x > 0.22$ such 100-Å-thick films are safely in the uniform long-range F phase [32–34]. The *only* significant difference between $x = 0.50$ and 0.28 films (including the magnetostriction, which is similar at these x [52]) is then the diminished V_O order (Fig. 4(f)), which has a major impact on PMA (Fig. 4(b)). Note that while the differing bulk lattice parameters at $x = 0.50$ and 0.28 does lead to slightly different strains in the two cases, this amounts to only 0.2% difference. Neither the magnetostrictions nor their x dependence in this composition range [52] are large enough (by one order of magnitude) to account for the significant difference in PMA between Fig. 4(a) and Fig. 4(b) based on only 0.2% strain difference. x-dependent data are thus crucial in establishing a definitive link between V_O order and PMA, as opposed to other potential origins.

The picture we thus advance is that the OVO superlattice, whether in- or out-of-plane, generates a uniaxial magnetic anisotropy perpendicular to oxygen-deficient planes. The x = 0.5 films in Fig. 4(e) are thus essentially a unit-cell-level superlattice of oxygen-sufficient/oxygen-deficient planes, with maximal interfacial density. When these features orient in the plane of the substrate/film interface, under compression, this results in PMA, the V_O interfacial anisotropy overcoming the magnetocrystalline anisotropy and in-plane demagnetizing field. While establishing the exact origin of this new anisotropy will require further work, particularly theory, it is likely that interfaces between oxygen-deficient tetrahedrally-coordinated and oxygen-sufficient octahedrally-coordinated Co are critical. This suggests clear parallels with other PMA systems, such as transition metal/MgO interfaces, where interfacial bonding is key [42], as well as metallic superlattices such as Co/Pt [41,53–55], Co/Pd [41,53], and Co/Ni [41,56]. PMA in the latter requires ultra-short superlattice periods (*i.e.*, high interface density) [41,53–56], analogous to single-unit-cell OVO superstructures. As a final comment, we note that recent work on $La_{1-x}Sr_xMnO_3/SrIrO_3$ superlattices reported PMA promoted by specific Ir-O-Mn interface bond angles [57], potentially relevant to the octahedral/tetrahedral interfaces mentioned above. Notably, the anisotropy constants in the current work are near identical to those in ref. 57, despite the lack of heavy elements such as Ir in the current case.

In summary, control over the orientation of OVO superstructures in LSCO films afforded by V_O-order-mediated lattice mismatch accommodation has been shown to enable precise control of magnetic anisotropy. In particular, in-plane V_O ordering induced by compressive strain generates strong PMA (6×10^6 erg/cm^3), a rarity in perovskites. The PMA is independent of thickness, ruling out surface and/or film/substrate interface anisotropies, but closely correlated with lateral coherence of defect ordering from STEM. This highlights the key role for the unit-

cell-level superlattice associated with the V_O order, raising intriguing analogies with metallic multilayers. Generally, this work highlights the significant potential for engineering V_O order to control function in complex oxide films and heterostructures.

Acknowledgments: Work primarily supported by the US Department of Energy through the University of Minnesota (UMN) Center for Quantum Materials, under DE-FG02-06ER46275 and DE-SC-0016371. Parts of this work were carried out in the Characterization Facility, UMN, which receives partial support from NSF through the MRSEC program. This research also used resources of the Advanced Photon Source, a DOE Office of Science User Facility operated by Argonne National Laboratory under DE-AC02-06CH11357. Electron microscopy observations were carried out at the Centro Nacional de Microscopía Electrónica (UCM, Spain). Financial support from the Spanish MINECO/FEDER through grant No. MAT2015-066888-C3-3-R is acknowledged by M.V. and M.C..

REFERENCES

[1] R. Ramesh and D. G. Schlom, Whither oxide electronics?, MRS Bull. **33**, 1006 (2008).

[2] J. H. Ngai, F. J. Walker, and C. H. Ahn, Correlated oxide physics and electronics, Annu. Rev. Mater. Res. **44**, 1 (2014).

[3] J. A. Sulpizio, S. Ilani, P. Irvin, and J. Levy, Nanoscale phenomena in oxide heterostructures, Annu. Rev. Mater. Res. **44**, 117 (2014).

[4] A. Bhattacharya and S. J. May, Magnetic oxide heterostructures, Annu. Rev. Mater. Res. **44**, 65 (2014).

[5] H. Y. Hwang, Y. Iwasa, M. Kawasaki, B. Keimer, N. Nagaosa, and Y. Tokura, Emergent phenomena at oxide interfaces, Nat. Mater. **11**, 103 (2012).

[6] S. Stemmer and S. James Allen, Two-dimensional electron gases at complex oxide interfaces, Annu. Rev. Mater. Res. **44**, 151 (2014).

[7] D. G. Schlom, L.-Q. Chen, C.-B. Eom, K. M. Rabe, S. K. Streiffer, and J.-M. Triscone, Strain tuning of ferroelectric thin films, Annu. Rev. Mater. Res. **37**, 589 (2007).

[8] J. H. Haeni, P. Irvin, W. Chang, R. Uecker, P. Reiche, Y. L. Li, S. Choudhury, W. Tian, M. E. Hawley, B. Craigo, A. K. Tagantsev, X. Q. Pan, S. K. Streiffer, L. Q. Chen, S. W. Kirchoefer, J. Levy, and D. G. Schlom, Room-temperature ferroelectricity in strained $SrTiO_3$, Nature **430**, 758 (2004).

[9] C. H. Ahn, A. Bhattacharya, M. Di Ventra, J. N. Eckstein, C. D. Frisbie, M. E. Gershenson, A. M. Goldman, I. H. Inoue, J. Mannhart, A. J. Millis, A. F. Morpurgo, D. Natelson, and J.-M. Triscone, Electrostatic modification of novel materials, Rev. Mod. Phys. **78**, 1185 (2006).

[10] S. Z. Bisri, S. Shimizu, M. Nakano, and Y. Iwasa, Endeavor of iontronics: From fundamentals to applications of ion-controlled electronics, Adv. Mater. **29**, 1607054 (2017).

[11] H. Jeen, W. S. Choi, J. W. Freeland, H. Ohta, C. U. Jung, and H. N. Lee, Topotactic phase transformation of the brownmillerite $SrCoO_{2.5}$ to the perovskite $SrCoO_{3-\delta}$, Adv. Mater. **25**, 3651 (2013).

[12] H. Jeen, W. S. Choi, M. D. Biegalski, C. M. Folkman, I.-C. Tung, D. D. Fong, J. W. Freeland, D. Shin, H. Ohta, M. F. Chisholm, and H. N. Lee, Reversible redox reactions in an epitaxially stabilized $SrCoO_x$ oxygen sponge, Nat. Mater. **12**, 1057 (2013).

[13] A. Spinelli, M. A. Torija, C. Liu, C. Jan, and C. Leighton, Electronic transport in doped $SrTiO_3$: Conduction mechanisms and potential applications, Phys. Rev. B **81**, 155110 (2010).

[14] W. D. Rice, P. Ambwani, M. Bombeck, J. D. Thompson, G. Haugstad, C. Leighton, and S. A. Crooker, Persistent optically induced magnetism in oxygen-deficient strontium titanate, Nat. Mater. **13**, 481 (2014).

[15] K. Ganguly, A. Prakash, B. Jalan, and C. Leighton, Mobility-electron density relation probed via controlled oxygen vacancy doping in epitaxial $BaSnO_3$, APL Mater. **5**, 056102 (2017).

[16] Y. Xie, M. D. Scafetta, R. J. Sichel-Tissot, E. J. Moon, R. C. Devlin, H. Wu, A. L. Krick, and S. J. May, Control of functional responses via reversible oxygen loss in $La_{1-x}Sr_xFeO_{3-\delta}$

films, Adv. Mater. **26**, 1434 (2014).

[17] N. Lu, P. Zhang, Q. Zhang, R. Qiao, Q. He, H.-B. Li, Y. Wang, J. Guo, D. Zhang, Z. Duan, Z. Li, M. Wang, S. Yang, M. Yan, E. Arenholz, S. Zhou, W. Yang, L. Gu, C.-W. Nan, J. Wu, Y. Tokura, and P. Yu, Electric-field control of tri-state phase transformation with a selective dual-ion switch, Nature **546**, 124 (2017).

[18] M. Li, W. Han, X. Jiang, J. Jeong, M. G. Samant, and S. S. P. Parkin, Suppression of ionic liquid gate-induced metallization of $SrTiO_3$(001) by oxygen, Nano Lett. **13**, 4675 (2013).

[19] J. Walter, G. Yu, B. Yu, A. Grutter, B. Kirby, J. Borchers, Z. Zhang, H. Zhou, T. Birol, M. Greven, and C. Leighton, Ion-gel-gating-induced oxygen vacancy formation in epitaxial $La_{0.5}Sr_{0.5}CoO_{3-\delta}$ films from in operando x-ray and neutron scattering, Phys. Rev. Mater. **1**, 071403(R) (2017).

[20] J. Walter, H. Wang, B. Luo, C. D. Frisbie, and C. Leighton, Electrostatic versus electrochemical doping and control of ferromagnetism in ion-gel-gated ultrathin $La_{0.5}Sr_{0.5}CoO_{3-\delta}$, ACS Nano **10**, 7799 (2016).

[21] A. Nemudry, P. Rudolf, and R. Schöllhorn, Topotactic electrochemical redox reactions of the defect perovskite $SrCoO_{2.5+x}$, Chem. Mater. **8**, 2232 (1996).

[22] Y. Ito, R. F. Klie, N. D. Browning, and T. J. Mazanec, Atomic resolution analysis of the defect chemistry and microdomain structure of brownmillerite-type strontium cobaltite, J. Am. Ceram. Soc. **85**, 969 (2004).

[23] C. K. Xie, Y. F. Nie, B. O. Wells, J. I. Budnick, W. A. Hines, and B. Dabrowski, Magnetic phase separation in $SrCoO_x$ ($2.5 \leq x \leq 3$), Appl. Phys. Lett. **99**, 052503 (2011).

[24] W. Paulus, H. Schober, S. Eibl, M. Johnson, T. Berthier, O. Hernandez, M. Ceretti, M. Plazanet, K. Conder, and C. Lamberti, Lattice dynamics to trigger low temperature oxygen mobility in solid oxide ion conductors, J. Am. Chem. Soc. **130**, 16080 (2008).

[25] Y. Long, Y. Kaneko, S. Ishiwata, Y. Taguchi, and Y. Tokura, Synthesis of cubic $SrCoO_3$ single crystal and its anisotropic magnetic and transport properties, J. Phys. Condens. Matter **23**, 245601 (2011).

[26] Q. Lu and B. Yildiz, Voltage-controlled topotactic phase transition in thin-film $SrCoO_x$ monitored by in situ x-ray diffraction, Nano Lett. **16**, 1186 (2016).

[27] J. Gazquez, S. Bose, M. Sharma, M. A. Torija, S. J. Pennycook, C. Leighton, and M. Varela, Lattice mismatch accommodation via oxygen vacancy ordering in epitaxial $La_{0.5}Sr_{0.5}CoO_{3-\delta}$ thin films, APL Mater. **1**, 012105 (2013).

[28] M. A. Torija, M. Sharma, J. Gazquez, M. Varela, C. He, J. Schmitt, J. A. Borchers, M. Laver, S. El-Khatib, and C. Leighton, Chemically driven nanoscopic magnetic phase separation at the $SrTiO_3$(001)/$La_{1-x}Sr_xCoO_3$ interface, Adv. Mater. **23**, 2711 (2011).

[29] D. O. Klenov, W. Donner, B. Foran, and S. Stemmer, Impact of stress on oxygen vacancy ordering in epitaxial $(La_{0.5}Sr_{0.5})CoO_{3-\delta}$ thin films, Appl. Phys. Lett. **82**, 3427 (2003).

[30] X. Wu, J. Walter, T. Feng, J. Zhu, H. Zheng, J. F. Mitchell, N. Biškup, M. Varela, X. Ruan, C. Leighton, and X. Wang, Glass-like through-plane thermal conductivity induced by oxygen vacancies in nanoscale epitaxial $La_{0.5}Sr_{0.5}CoO_{3-\delta}$, Adv. Funct. Mater. **27**, 1704233 (2017).

[31] M. A. Torija, M. Sharma, M. R. Fitzsimmons, M. Varela, and C. Leighton, Epitaxial $La_{0.5}Sr_{0.5}CoO_3$ thin films: Structure, magnetism, and transport, J. Appl. Phys. **104**, 023901

(2008).

[32] J. Wu and C. Leighton, Glassy ferromagnetism and magnetic phase separation in $La_{1-x}Sr_xCoO_3$, Phys. Rev. B **67**, 174408 (2003).

[33] J. Wu, J. W. Lynn, C. J. Glinka, J. Burley, H. Zheng, J. F. Mitchell, and C. Leighton, Intergranular giant magnetoresistance in a spontaneously phase separated perovskite oxide, Phys. Rev. Lett. **94**, 037201 (2005).

[34] C. He, S. El-Khatib, J. Wu, J. W. Lynn, H. Zheng, J. F. Mitchell, and C. Leighton, Doping fluctuation-driven magneto-electronic phase separation in $La_{1-x}Sr_xCoO_3$ single crystals, Europhys. Lett. **87**, 27006 (2009).

[35] M. Sharma, J. Gazquez, M. Varela, J. Schmitt, and C. Leighton, Coercivity enhancement driven by interfacial magnetic phase separation in SrTiO3(001)/$Nd_{0.5}Sr_{0.5}CoO_3$, Phys. Rev. B **84**, 024417 (2011).

[36] D. Fuchs, E. Arac, C. Pinta, S. Schuppler, R. Schneider, and H. v. Löhneysen, Tuning the magnetic properties of $LaCoO_3$ thin films by epitaxial strain, Phys. Rev. B **77**, 014434 (2008).

[37] C. Xie, J. I. Budnick, B. O. Wells, and J. C. Woicik, Separation of the strain and finite size effect on the ferromagnetic properties of $La_{0.5}Sr_{0.5}CoO_3$ thin films, Appl. Phys. Lett. **91**, 172509 (2007).

[38] R. C. O'Handley, *Modern Magnetic Materials - Principles and Applications* (Wiley & Sons, New York, 2000).

[39] J. Mira, J. Rivas, M. Vázquez, M. R. Ibarra, R. Caciuffo, and M. A. Señarís Rodríguez, Field-induced magnetic anisotropy in $La_{0.7}Sr_{0.3}CoO_3$, Europhys. Lett. **62**, (2003).

[40] H. M. Aarbogh, J. Wu, L. Wang, H. Zheng, J. F. Mitchell, and C. Leighton, Magnetic and electronic properties of $La_{1-x}Sr_xCoO_3$ single crystals across the percolation metal-insulator transition, Phys. Rev. B **74**, 134408 (2006).

[41] F. Hellman, A. Hoffmann, Y. Tserkovnyak, G. S. D. Beach, E. E. Fullerton, C. Leighton, A. H. MacDonald, D. C. Ralph, D. A. Arena, H. A. Dürr, P. Fischer, J. Grollier, J. P. Heremans, T. Jungwirth, A. V Kimel, B. Koopmans, I. N. Krivorotov, S. J. May, A. K. Petford-Long, J. M. Rondinelli, N. Samarth, I. K. Schuller, A. N. Slavin, M. D. Stiles, O. Tchernyshyov, A. Thiaville, and B. L. Zink, Interface-induced phenomena in magnetism, Rev. Mod. Phys. **89**, 025006 (2017).

[42] B. Dieny and M. Chshiev, Perpendicular magnetic anisotropy at transition metal/oxide interfaces and applications, Rev. Mod. Phys. **89**, 025008 (2017).

[43] J. Walter, T. Charlton, H. Ambaye, M. R. Fitzsimmons, P. P. Orth, R. M. Fernandes, and C. Leighton, Giant electrostatic modification of mgnetism via electrolyte-gate-induced cluster percolation in $La_{1-x}Sr_xCoO_{3-\delta}$, arXiv: 1807.09364.

[44] S. Bose, M. Sharma, M. A. Torija, J. Gazquez, M. Varela, H. Ambaye, R. Goyette, V. Lauter, M. Zhernenkov, M. R. Fitzsimmons, O. Hovorka, A. Berger, J. Schmitt, and C. Leighton, (unpublished).

[45] Y.-M. Kim, J. He, M. D. Biegalski, H. Ambaye, V. Lauter, H. M. Christen, S. T. Pantelides, S. J. Pennycook, S. V. Kalinin, and A. Y. Borisevich, Probing oxygen vacancy concentration and homogeneity in solid-oxide fuel-cell cathode materials on the subunit-cell level, Nat. Mater. **11**, 888 (2012).

[46] V. V. Mehta, N. Biskup, C. Jenkins, E. Arenholz, M. Varela, and Y. Suzuki, Long-range ferromagnetic order in $LaCoO_{3-\delta}$ epitaxial films due to the interplay of epitaxial strain and oxygen vacancy ordering, Phys. Rev. B **91**, 144418 (2015).

[47] N. Biškup, J. Salafranca, V. Mehta, M. P. Oxley, Y. Suzuki, S. J. Pennycook, S. T. Pantelides, and M. Varela, Insulating ferromagnetic $LaCoO_{3-\delta}$ films: A phase induced by ordering of oxygen vacancies, Phys. Rev. Lett. **112**, 087202 (2014).

[48] H. W. Yang, H. R. Zhang, Y. Li, S. F. Wang, X. Shen, Q. Q. Lan, S. Meng, R. C. Yu, B. G. Shen, and J. R. Sun, Anomalous magnetism in strained $La_{1-x}Sr_xCoO_3$ epitaxial films ($0 \leq x \leq 0.5$), Sci. Rep. **4**, 6206 (2015).

[49] C. Kwon, M. C. Robson, K.-C. Kim, J. Y. Gu, S. E. Lofland, S. M. Bhagat, Z. Trajanovic, M. Rajeswari, T. Venkatesan, a. R. Kratz, R. D. Gomez, and R. Ramesh, Stress-induced effects in epitaxial $(La_{0.7}Sr_{0.3})MnO_3$ films, J. Magn. Magn. Mater. **172**, 229 (1997).

[50] F. Tsui, M. C. Smoak, T. K. Nath, and C. B. Eom, Strain-dependent magnetic phase diagram of epitaxial $La_{0.67}Sr_{0.33}MnO_3$ thin films, Appl. Phys. Lett. **76**, 2421 (2000).

[51] G. Srinivasan, E. T. Rasmussen, B. J. Levin, and R. Hayes, Magnetoelectric effects in bilayers and multilayers of magnetostrictive and piezoelectric perovskite oxides, Phys. Rev. B **65**, 134402 (2002).

[52] M. R. Ibarra, R. Mahendiran, C. Marquina, B. García-Landa, and J. Blasco, Huge anisotropic magnetostriction in $La_{1-x}Sr_xCoO_3$ ($x \geq 0.3$): Field-induced orbital instability, Phys. Rev. B **57**, R3217 (1998).

[53] P. F. Carcia, Perpendicular magnetic anisotropy in Pd/Co and Pt/Co thin□film layered structures, J. Appl. Phys. **63**, 5066 (1988).

[54] B. N. Engel, C. D. England, R. A. Van Leeuwen, M. H. Wiedmann, and C. M. Falco, Interface magnetic anisotropy in epitaxial superlattices, Phys. Rev. Lett. **67**, 1910 (1991).

[55] J. E. Davies, O. Hellwig, E. E. Fullerton, G. Denbeaux, J. B. Kortright, and K. Liu, Magnetization reversal of Co/Pt multilayers: Microscopic origin of high-field magnetic irreversibility, Phys. Rev. B **70**, 224434 (2004).

[56] G. H. O. Daalderop, P. J. Kelly, and F. J. A. den Broeder, Prediction and confirmation of perpendicular magnetic anisotropy in Co/Ni multilayers, Phys. Rev. Lett. **68**, 682 (1992).

[57] D. Yi, C.L. Flint, P. P. Blakrishnan, K. Mahalingam, B. Urwin, A. Vailionis, A. T. N'Diaye, P. Shafer, E. Arenholz, Y. Choi, K.H. Stone, J.-H. Chu, B.M. Howe, J. Liu, I. R. Fisher and Y. Suzuki, Tuning perpendicular magnetic anisotropy by oxygen octahedral rotations in $(La_{1-x}Sr_xMnO_3)/(SrIrO_3)$ superlattices, Phys. Rev. Lett. **119**, 077201 (2017).

FIGURE CAPTIONS

Fig. 1. Schematic structures of fully oxygen-vacancy-ordered (brownmillerite) $La_{1-x}Sr_xCoO_3$ films under (a) tensile and (b) compressive lattice mismatch and strain (ε_{xx}). Shown are Co ions (green), La/Sr ions (blue), O ions (red), oxygen vacancies (white), and substrate ions (bottom, shaded black). Transparent polyhedra emphasize the O-stoichiometric (red) and O-deficient (gray) planes. Pseudocubic axes are shown.

Fig. 2. (a-d) Specular synchrotron wide-angle X-ray diffraction (intensity *vs*. out-of-plane scattering vector magnitude, Q) from 90-Å-thick $La_{0.5}Sr_{0.5}CoO_{3-\delta}$ (LSCO) films on 001-oriented $SrTiO_3$ (STO, purple), $La_{0.18}Sr_{0.82}Al_{0.59}Ta_{0.41}O_3$ (LSAT, blue), $LaAlO_3$ (LAO, red), and $SrLaAlO_4$ (SLAO, green). The 002 LSCO peak is marked with the black dashed line. (e) Out-of-plane strain (ε_{zz}) *vs*. in-plane lattice mismatch (ε_{xx}) for the films in (a-d), using a bulk LSCO lattice parameter of 3.833 Å. The red dashed line is the expectation for biaxial strain with Poisson ratio 1/3. (f) Asymmetric 013 reciprocal space map from 380-Å-thick LAO(001)/LSCO. Expected positions for LAO, fully-strained LSCO, and fully-relaxed LSCO are shown.

Fig. 3. Magnetometry on 90-Å-thick $La_{0.5}Sr_{0.5}CoO_{3-\delta}$ (LSCO) films on 001-oriented $SrTiO_3$ (STO, purple), $La_{0.18}Sr_{0.82}Al_{0.59}Ta_{0.41}O_3$ (LSAT, blue), $LaAlO_3$ (LAO, red), and $SrLaAlO_4$ (SLAO, green). (a-d) Temperature (T) dependence of magnetization (M) for out-of-plane (OoP, solid) and in-plane (IP, dashed) cooling and measuring magnetic fields, H = 1 kOe. (e-h) M *vs.* H at 5 K for OoP (solid) and IP (dashed) orientations. In-plane lattice mismatch (ε_{xx}) dependence of: (i) Curie temperature (T_C), (j) 5 K coercivity (H_c), and (k) 5 K remnant magnetization normalized to saturation (M_r/M_s). (l-n) Thickness (t) dependence of T_C, 5 K H_c, and 5 K M_R/M_s, for LAO(001)/LSCO. The vertical dotted line marks the dead layer thickness, t_c. All

magnetometry data required careful subtraction of relatively large contributions from the substrate, sample holder, *etc*.

Fig. 4. 5 K Magnetization (*M*) *vs*. magnetic field (*H*) loops for out-of-plane (OoP, red) and in-plane (IP, black) orientations for ~100-Å-thick $La_{1-x}Sr_xCoO_{3-\delta}$ films on $LaAlO_3$(001) with *x* of (a) 0.5, (b) 0.28, (c) 0.15, and (d) 0.05. Corresponding *Z*-contrast scanning transmission electron microscopy images are shown in (e-h), in the pseudocubic [110] or [010] orientations. Red arrows mark oxygen deficient planes; blue arrows mark the film/substrate interface. All magnetometry data required careful subtraction of relatively large contributions from the substrate, sample holder, *etc*.

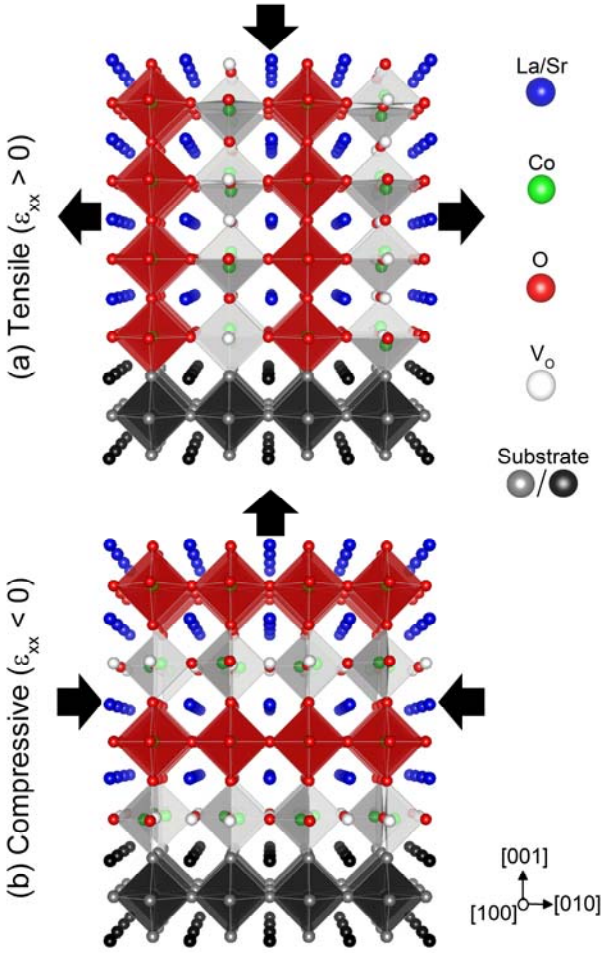
(a) Tensile (ε_{xx} > 0)
(b) Compressive (ε_{xx} < 0)
La/Sr
Co
O
V_o
Substrate
[001]
[100]
[010]

Figure 1

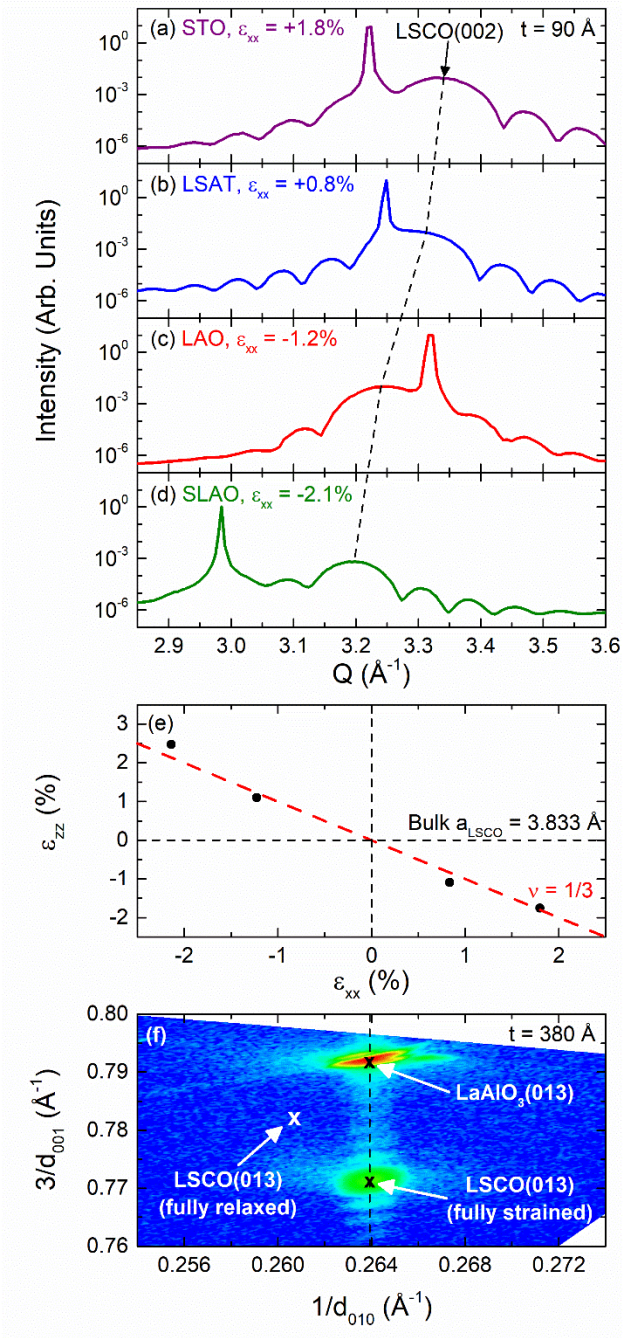
(a) STO, ε_xx = +1.8%
LSCO(002) t = 90 Å
(b) LSAT, ε_xx = +0.8%
(c) LAO, ε_xx = -1.2%
(d) SLAO, ε_xx = -2.1%
Intensity (Arb. Units)
Q (Å^-1)
(e)
Bulk a_LSCO = 3.833 Å
ν = 1/3
ε_zz (%)
ε_xx (%)
(f)
t = 380 Å
LaAlO3(013)
LSCO(013) (fully relaxed)
LSCO(013) (fully strained)
3/d_001 (Å^-1)
1/d_010 (Å^-1)

Figure 2

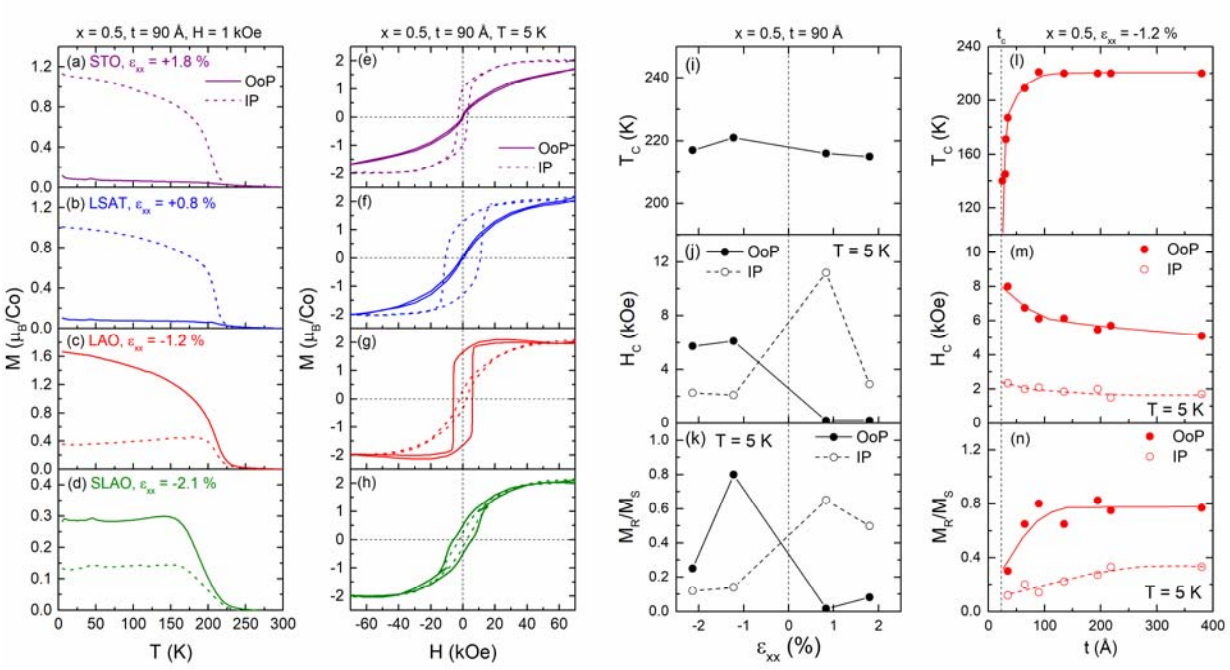
x = 0.5, t = 90 Å, H = 1 kOe
(a) STO, ε_xx = +1.8 %
OoP
IP
(b) LSAT, ε_xx = +0.8 %
(c) LAO, ε_xx = -1.2 %
(d) SLAO, ε_xx = -2.1 %
M (μ_B/Co)
T (K)
x = 0.5, t = 90 Å, T = 5 K
(e)
(f)
(g)
(h)
H (kOe)
x = 0.5, t = 90 Å
(i)
T_C (K)
(j)
T = 5 K
H_C (kOe)
(k)
M_R/M_S
ε_xx (%)
t_c
x = 0.5, ε_xx = -1.2 %
(l)
(m)
(n)
t (Å)

Figure 3

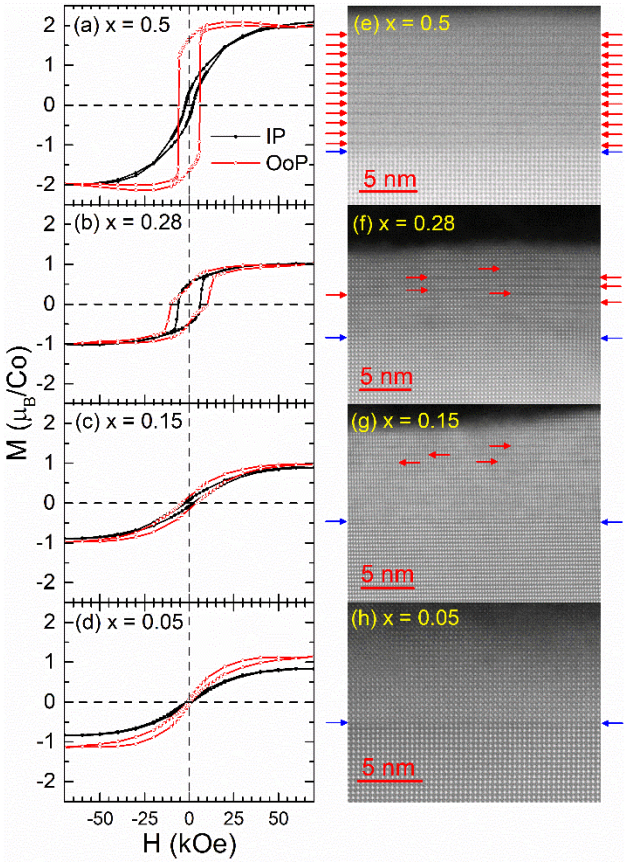
(a) x = 0.5
IP
OoP
(b) x = 0.28
(c) x = 0.15
(d) x = 0.05
M (μ_B/Co)
H (kOe)
(e) x = 0.5
5 nm
(f) x = 0.28
5 nm
(g) x = 0.15
5 nm
(h) x = 0.05
5 nm

Figure 4